Linear dispersion properties of ring velocity distribution functions

Marek Vandas[1,*] and Petr Hellinger[1,2]

[1] *Astronomical Institute, AS CR, Bocni II/1401, CZ-14100 Prague, Czech Republic*
[2] *Institute of Atmospheric Physics, AS CR, Bocni II/1401, CZ-14100 Prague, Czech Republic*

(Dated: May 22, 2015)

Linear properties of ring velocity distribution functions are investigated. The dispersion tensor in a form similar to the case of a Maxwellian distribution function, but for a general distribution function separable in velocities, is presented. Analytical forms of the dispersion tensor are derived for two cases of ring velocity distribution functions: one obtained from physical arguments and one for the usual, ad hoc ring distribution. The analytical expressions involve generalized hypergeometric, Kampé de Fériet functions of two arguments. For a set of plasma parameters the two ring distribution functions are compared. At the parallel propagation with respect to the ambient magnetic field the two ring distributions give the same results identical to the corresponding bi-Maxwellian distribution. At oblique propagation the two ring distributions give similar results only for strong instabilities whereas for weak growth rates their predictions are significantly different; the two ring distributions have different marginal stability conditions.

I. INTRODUCTION

Injection of newly ionized, pickup neutral particles which moved with respect to the ambient plasma generally leads to a nongyrotropic particle velocity distribution function. Nongyrotropic distribution functions appear in cometary environments[1] and exhibit complicated linear properties.[2] When the (spatial and temporal) scales of the source are much larger than the particle gyroperiod/gyroradius, the generated pickup distribution function has a form of a ring-beam, i.e., a ring propagating with respect to the ambient plasma along the ambient magnetic field.[3] Many different types of pickup ions are ubiquitously observed in the solar wind[4] with interstellar or local origin. Pickup ions originating from the charge exchange between the solar wind ions and interstellar neutrals are important for an overall evolution of the solar wind in the outer heliosphere.[5,6] The hot neutrals of the solar wind origin may undergo further charge-exchange processes and are likely a source of energetic neutrals observed in the inner heliosphere.[7] In one of the generating scenario,[8,9] the hot neutrals undergo a charge exchange in the outer heliosheath forming a ring distribution. An additional charge exchange may produce energetic neutrals with properties consistent with the observed features if the original ring distribution is stable enough. In weakly collisional plasmas the ring distributions may be a source of free energy for many different instabilities, e.g., due to effective temperature anisotropies and/or due to differential streaming.[10–13]

The ring-beam distribution f_r is often assumed to be cold:[8,12,14]

$$f_r(v_\parallel, v_\perp) \propto \frac{1}{2\pi v_\perp}\delta(v_\parallel - v_{\parallel 0})\delta(v_\perp - v_{\perp 0}); \qquad (1)$$

here $v_\parallel$ and $v_\perp$ denote parallel and perpendicular velocities with respect the ambient magnetic field, and $v_{\parallel 0}$ and $v_{\perp 0}$ are the parallel and perpendicular injection velocities. This form is, however, not generally applicable (the effective temperature anisotropy of this distribution is infinite). For a hot ring population the following form of the velocity distribution function is usually used:[9,15,16]

$$f_r(v_\parallel, v_\perp) \propto \mathrm{e}^{-\frac{(v_\perp - v_{\perp 0})^2}{2v_{\rm th}^2} - \frac{(v_\parallel - v_{\parallel 0})^2}{2v_{\rm th}^2}} \qquad (2)$$

where $v_{\rm th}$ denotes an equivalent of the thermal velocity. Presence of a finite thermal spread tends to stabilize the system[9]. One should note, however, that the distribution (2) has an ad hoc form. As we shall see below, natural physical arguments lead to a different ring distribution with different stability properties.

In the present paper we derive a new ring distribution function (called "ring distribution 1" herein) based on physical arguments and derive new, analytical forms of dispersion relations for this distribution as well as for the usual ad hoc one (called "ring distribution 2" herein, Eq. (2)). The analytical forms enable a more flexible investigation of linear dispersion properties of ring distribution functions in contrast to the typical numerical approach using numerical integration.[15,16] The paper is organized as follows: In Section II we derive the physics-based ring distribution function (ring distribution 1). In the beginning of Section III we analyze general properties of distribution functions which are separable in velocities. In Sections III D and III E we derive analytical forms of dispersion relations for ring distribution functions 1 and 2, respectively. In Section IV we compare linear properties of the two ring distributions (as well as linear properties of a corresponding anisotropic bi-Maxwellian distribution) for a few choices of plasma parameters. Finally, in Section V we discuss the obtained results followed by utilized mathematical expressions in Appendices A–F.

II. NATURAL RING DISTRIBUTION FUNCTION

Let us first derive a ring-beam velocity distribution function from physical arguments. We suppose a homogeneous neutral particle population with

a Maxwellian velocity distribution function ($v_{\rm th}$ being its thermal velocity) which propagates with a velocity $(v_{0\perp}\cos\phi, v_{0\perp}\sin\phi, v_{0\parallel})$ with respect to the (Cartesian) plasma rest frame. Here we consider the ambient magnetic field to be along the z axis, $\boldsymbol{B} = (0, 0, B_0)$, so $v_{0\parallel}$ is the particle velocity along the ambient magnetic field, and $v_{0\perp}$ is perpendicular to it with the phase ϕ. If we assume that these neutrals are ionized by a process which is independent of their velocity, the injected ions have a velocity distribution (in v_x, v_y, and v_z)

$$f_{\rm inj} \propto {\rm e}^{-\frac{(v_x - v_{0\perp}\cos\phi)^2 + (v_y - v_{0\perp}\sin\phi)^2 + (v_z - v_{0\parallel})^2}{2v_{\rm th}^2}}. \quad (3)$$

The newly born ions immediately start to gyrate around the ambient magnetic field. If the injection continues over a time much larger than the gyration time with a constant injection rate, the resulting velocity distribution function is given as

$$f_r \propto \frac{1}{2\pi}{\rm e}^{-\frac{(v_z - v_{0\parallel})^2}{2v_{\rm th}^2}} \int_0^{2\pi} {\rm e}^{-\frac{(v_x - v_{0\perp}\cos\phi)^2 + (v_y - v_{0\perp}\sin\phi)^2}{2v_{\rm th}^2}} {\rm d}\phi \quad (4)$$

which leads to

$$f_r \propto {\rm e}^{-\frac{v_\perp^2 + v_{0\perp}^2}{2v_{\rm th}^2}} I_0\left(\frac{v_\perp v_{0\perp}}{v_{\rm th}^2}\right) {\rm e}^{-\frac{(v_z - v_{0\parallel})^2}{2v_{\rm th}^2}} \quad (5)$$

where I_0 is the Bessel function of the second kind. The natural ring-beam distribution function (5) is clearly different from the ad hoc form (2). While for a wide range of parameters the two distributions look similar, they likely have different linear properties, especially for resonant instabilities which depend strongly on details of a distribution function.[17] Here we investigate linear dispersion properties of the two ring distributions. Both of them are separable in velocities (i.e., their distribution function $f(v_\parallel, v_\perp)$ can be given as $f(v_\parallel, v_\perp) \propto f_\parallel(v_\parallel) f_\perp(v_\perp)$) so that we start with a general case of such a distribution function.

III. DISPERSION TENSOR FOR A SEPARABLE DISTRIBUTION FUNCTION

The dispersion tensor $\mathbf{D}$ for a plasma consisting of a set of species (denoted by the subscript s) with general gyrotropic distribution functions $f_{\rm s}(v_\parallel, v_\perp)$ is given by

$$\mathbf{D} = \left(1 - \frac{k^2c^2}{\omega^2}\right)\mathbf{1} + \frac{c^2}{\omega^2}\boldsymbol{kk} + \sum_{\rm s}\frac{\omega_{ps}^2}{\omega^2}\mathbf{Q}_{\rm s} \quad (6)$$

with[18]

$$\mathbf{Q}_{\rm s} = \sum_{n=-\infty}^{\infty}\int\left(k_\parallel\frac{\partial f_{\rm s}}{\partial v_\parallel} + n\frac{\omega_{cs}}{v_\perp}\frac{\partial f_{\rm s}}{\partial v_\perp}\right) \times \frac{\mathbf{T}_{ns}}{\omega - k_\parallel v_\parallel - n\omega_{cs}}{\rm d}^3\boldsymbol{v} - \mathbf{1}, \quad (7)$$

$$\mathbf{T}_{ns} = \begin{pmatrix} \frac{n^2\omega_{cs}^2}{k_\perp^2}J_n^2 & \frac{in\omega_{cs}}{k_\perp}v_\perp J_n J_n' & \frac{n\omega_{cs}}{k_\perp}v_\parallel J_n^2 \\ -\frac{in\omega_{cs}}{k_\perp}v_\perp J_n J_n' & v_\perp^2 J_n'^2 & -iv_\parallel v_\perp J_n J_n' \\ \frac{n\omega_{cs}}{k_\perp}v_\parallel J_n^2 & iv_\parallel v_\perp J_n J_n' & v_\parallel^2 J_n^2 \end{pmatrix}. \quad (8)$$

Here J_n and J_n' are the Bessel functions of the first kind and their derivatives, respectively, of the integer order n and the argument $k_\perp v_\perp/\omega_{cs}$; $\omega_{ps} = [q_{\rm s}^2 n_{\rm s}/(m_{\rm s}\varepsilon_0)]^{1/2}$ and $\omega_{cs} = q_{\rm s}B_0/m_{\rm s}$ are the plasma and cyclotron frequencies of the species s, respectively. The ambient magnetic field is homogeneous and along the z axis, $\boldsymbol{B}_0 = (0, 0, B_0)$. The species s has the mass $m_{\rm s}$, charge $q_{\rm s}$, number density $n_{\rm s}$, and the distribution function $f_{\rm s}$ which is considered as a function of parallel ($v_\parallel$) and perpendicular ($v_\perp$) velocities with respect to the ambient magnetic field only. The expression (8) is written for the wave vector $\boldsymbol{k} = (k_\perp, 0, k_\parallel)$, ω is the complex wave frequency, i is the imaginary unit, ε_0 and c are the permittivity and speed of light, respectively, in vacuum.

Let us assume that the distribution function $f_{\rm s}$ is separable in velocities, i.e., it has the form

$$f_{\rm s}(v_\parallel, v_\perp) = \frac{1}{(2\pi)^{\frac{3}{2}}w_{\rm s\parallel}w_{\rm s\perp}^2}f_{\rm s\parallel}(v_\parallel)f_{\rm s\perp}(v_\perp) \quad (9)$$

where

$$w_{\rm s\parallel} = \frac{1}{\sqrt{2\pi}}\int_{-\infty}^{\infty} f_{\rm s\parallel}(v_\parallel)\,{\rm d}v_\parallel, \quad (10)$$

$$w_{\rm s\perp} = \left[\int_0^{\infty} v_\perp f_{\rm s\perp}(v_\perp)\,{\rm d}v_\perp\right]^{\frac{1}{2}}. \quad (11)$$

This form of the distribution function was selected to have an easy correspondence with results on Maxwellian distributions. The distribution function is normalized to unity, i.e.,

$$\int f_{\rm s}{\rm d}^3\boldsymbol{v} = 2\pi\int_{-\infty}^{\infty}\int_0^{\infty} v_\perp f_{\rm s}(v_\parallel, v_\perp)\,{\rm d}v_\perp\,{\rm d}v_\parallel = 1, \quad (12)$$

the physical distribution function is $n_{\rm s}f_{\rm s}$.

Calculating the tensor $\mathbf{Q}_{\rm s}$ for our case, it is useful to define integrals

$$R_{nmj}^{({\rm s})} = \frac{k_\parallel^m w_{\rm s\parallel}^{m-j-1}}{\sqrt{\pi}}\int_{-\infty}^{\infty}\frac{v_\parallel^j}{(k_\parallel v_\parallel + n\omega_{cs} - \omega)^m}f_{\rm s\parallel}(v_\parallel)\,{\rm d}v_\parallel \quad (13)$$

and

$$S_{nmj}^{({\rm s})} = \frac{2}{(2w_{\rm s\perp}^2)^{\frac{j+1}{2}}} \times \int_0^{\infty} v_\perp^j J_n\left(\frac{k_\perp v_\perp}{\omega_{cs}}\right) J_m\left(\frac{k_\perp v_\perp}{\omega_{cs}}\right) f_{\rm s\perp}(v_\perp)\,{\rm d}v_\perp \quad (14)$$

where n, m, and $j \geq 0$ are integers. $R^{(\mathrm{s})}_{nmj}$ is defined by Eq. (13) for $\mathrm{Im}\,\omega > 0$. For other values its analytic continuation must be considered. Some properties of $R^{(\mathrm{s})}_{nmj}$ and $S^{(\mathrm{s})}_{nmj}$ are given in Appendix A.

A. General case

The tensor $\mathbf{Q}_\mathrm{s}$ can be written in the form

$$\mathbf{Q}_\mathrm{s} = \begin{pmatrix} -1 & 0 & \frac{k_\perp}{k_\parallel} \\ 0 & -1 & 0 \\ \frac{k_\perp}{k_\parallel} & 0 & -\frac{k_\perp^2}{k_\parallel^2} \end{pmatrix} + a_\mathrm{s} \sum_{n=-\infty}^{\infty} \begin{pmatrix} \frac{n^2}{l_\mathrm{s}^2} V_{1sn} & inV_{2sn} & \frac{n}{l_\mathrm{s}} y_{sn} V_{1sn} \\ -inV_{2sn} & V_{3sn} & -il_\mathrm{s} y_{sn} V_{2sn} \\ \frac{n}{l_\mathrm{s}} y_{sn} V_{1sn} & il_\mathrm{s} y_{sn} V_{2sn} & y_{sn}^2 V_{1sn} \end{pmatrix} \tag{15}$$

where

$$a_\mathrm{s} = \frac{w_{\mathrm{s}\perp}^2}{w_{\mathrm{s}\parallel}^2}, \quad l_\mathrm{s} = \frac{k_\perp w_{\mathrm{s}\perp}}{\omega_{\mathrm{cs}}}, \quad y_{sn} = \frac{\omega - n\omega_{\mathrm{cs}}}{k_\parallel w_{\mathrm{s}\perp}};$$

V_{1sn}, V_{2sn}, and V_{3sn} are expressed via integrals (13)–(14)

$$\begin{aligned} V_{1sn} &= -\frac{1}{\sqrt{2}} \sigma_{1sn} R^{(\mathrm{s})}_{n20} + n\mu_\mathrm{s} \sigma_{2sn} R^{(\mathrm{s})}_{n10}, \\ V_{2sn} &= \frac{1}{\sqrt{2} l_\mathrm{s}} \left(-\frac{1}{\sqrt{2}} \sigma_{3sn} R^{(\mathrm{s})}_{n20} + n\mu_\mathrm{s} \sigma_{8sn} R^{(\mathrm{s})}_{n10} \right), \\ V_{3sn} &= \frac{1}{2} \left(-\frac{1}{\sqrt{2}} \sigma_{7sn} R^{(\mathrm{s})}_{n20} + n\mu_\mathrm{s} \sigma_{9sn} R^{(\mathrm{s})}_{n10} \right), \end{aligned} \tag{16}$$

where $\mu_\mathrm{s} = k_\perp w_{\mathrm{s}\parallel} / (2k_\parallel w_{\mathrm{s}\perp})$ and

$$\begin{aligned} \sigma_{1sn} &= S^{(\mathrm{s})}_{nn1}, \\ \sigma_{2sn} &= S^{(\mathrm{s})}_{n-1,n,0} - S^{(\mathrm{s})}_{n,n+1,0}, \\ \sigma_{3sn} &= S^{(\mathrm{s})}_{n-1,n,2} - S^{(\mathrm{s})}_{n,n+1,2}, \\ \sigma_{4sn} &= S^{(\mathrm{s})}_{n-1,n-1,1} - 2S^{(\mathrm{s})}_{n-1,n+1,1} + S^{(\mathrm{s})}_{n+1,n+1,1}, \\ \sigma_{5sn} &= S^{(\mathrm{s})}_{n-2,n,1} + S^{(\mathrm{s})}_{n,n+2,1}, \\ \sigma_{6sn} &= S^{(\mathrm{s})}_{n-2,n-1,2} - S^{(\mathrm{s})}_{n-2,n+1,2} + S^{(\mathrm{s})}_{n-1,n+2,2} \\ &\quad - S^{(\mathrm{s})}_{n+1,n+2,2}, \\ \sigma_{7sn} &= S^{(\mathrm{s})}_{n-1,n-1,3} - 2S^{(\mathrm{s})}_{n-1,n+1,3} + S^{(\mathrm{s})}_{n+1,n+1,3}, \\ \sigma_{8sn} &= \frac{1}{2} \left(\frac{\sqrt{2}}{l_\mathrm{s}} \sigma_{2sn} + \sigma_{4sn} + \sigma_{5sn} - 2\sigma_{1sn} \right), \\ \sigma_{9sn} &= \frac{\sqrt{2}}{l_\mathrm{s}} \sigma_{4sn} + \sigma_{6sn} - 2\sigma_{3sn}. \end{aligned} \tag{17}$$

B. Streaming Maxwellian parallel distribution function

For the parallel distribution function

$$f_{\mathrm{s}\parallel}(v_\parallel) = \mathrm{e}^{-\frac{(v_\parallel - v_{0\mathrm{s}\parallel})^2}{2v_{\mathrm{s}\parallel}^2}} \tag{18}$$

the integrals (13) can be expressed via the plasma dispersion function[19] Z:

$$R^{(\mathrm{s})}_{n10} = Z(\xi_{sn}), \quad R^{(\mathrm{s})}_{n20} = -\sqrt{2}[1 + \xi_{sn} Z(\xi_{sn})] \tag{19}$$

where

$$\xi_{sn} = \frac{\omega - n\omega_{\mathrm{cs}} - k_\parallel v_{0\mathrm{s}\parallel}}{\sqrt{2} k_\parallel v_{\mathrm{s}\parallel}}. \tag{20}$$

It holds $w_{\mathrm{s}\parallel} = v_{\mathrm{s}\parallel}$, where $v_{\mathrm{s}\parallel}$ is the parallel thermal velocity related to the parallel temperature $T_{\mathrm{s}\parallel}$ by $v_{\mathrm{s}\parallel}^2 = k_B T_{\mathrm{s}\parallel}/m_\mathrm{s}$ (k_B is the Boltzmann constant), $v_{0\mathrm{s}\parallel}$ is the parallel streaming velocity.

The tensor $\mathbf{Q}_\mathrm{s}$ (15) yields in this specific case the form

$$\mathbf{Q}_\mathrm{s} = \begin{pmatrix} \tilde{A}_\mathrm{s} - 1 & 0 & (1 - \tilde{A}_\mathrm{s}) \frac{k_\perp}{k_\parallel} \\ 0 & \tilde{A}_\mathrm{s} - 1 & 0 \\ (1 - \tilde{A}_\mathrm{s}) \frac{k_\perp}{k_\parallel} & 0 & \frac{\omega^2}{k_\parallel^2 v_{\mathrm{s}\parallel}^2} + (\tilde{A}_\mathrm{s} - 1) \frac{k_\perp^2}{k_\parallel^2} \end{pmatrix} + a_\mathrm{s} \sum_{n=-\infty}^{\infty} Z(\xi_{sn}) \times \begin{pmatrix} \frac{n^2}{l_\mathrm{s}^2} K_{1sn} & inK_{2sn} & \frac{n}{l_\mathrm{s}} y_{sn} K_{1sn} \\ -inK_{2sn} & K_{3sn} & -il_\mathrm{s} y_{sn} K_{2sn} \\ \frac{n}{l_\mathrm{s}} y_{sn} K_{1sn} & il_\mathrm{s} y_{sn} K_{2sn} & y_{sn}^2 K_{1sn} \end{pmatrix} \tag{21}$$

where $\tilde{A}_\mathrm{s}$ is the effective temperature anisotropy,

$$\tilde{A}_\mathrm{s} = \frac{\int \frac{1}{2} v_\perp^2 f_\mathrm{s} \mathrm{d}^3 \boldsymbol{v}}{\int (v_\parallel - v_{0\mathrm{s}\parallel})^2 f_\mathrm{s} \mathrm{d}^3 \boldsymbol{v}} = \frac{1}{2 v_{\mathrm{s}\parallel}^2 w_{\mathrm{s}\perp}^2} \int_0^\infty v_\perp^3 f_{\mathrm{s}\perp} \mathrm{d}v_\perp, \tag{22}$$

and K_{1sn}, K_{2sn}, and K_{3sn} are defined as

$$\begin{aligned} K_{1sn} &= \xi_{sn} \sigma_{1sn} + n\mu_\mathrm{s} \sigma_{2sn}, \\ K_{2sn} &= \frac{1}{\sqrt{2} l_\mathrm{s}} (\xi_{sn} \sigma_{3sn} + n\mu_\mathrm{s} \sigma_{8sn}), \\ K_{3sn} &= \frac{1}{2} (\xi_{sn} \sigma_{7sn} + n\mu_\mathrm{s} \sigma_{9sn}); \end{aligned} \tag{23}$$

sums given in Appendix B were used during the derivation.

C. Streaming bi-Maxwellian distribution

Bi-Maxwellian distribution is a Maxwellian-like distribution where parallel and perpendicular temperatures (with respect to the ambient magnetic field) differ.[20] Its

parallel part is given by Eq. (18) and its perpendicular part has a similar form,

$$f_{\mathrm{s}\perp}(v_\perp) = \mathrm{e}^{-\frac{v_\perp^2}{2v_{\mathrm{s}\perp}^2}}, \tag{24}$$

where $v_{\mathrm{s}\perp}$ is the perpendicular thermal velocity. We introduce the temperature anisotropy

$$A_{\mathrm{s}} = \frac{v_{\mathrm{s}\perp}^2}{v_{\mathrm{s}\parallel}^2} \tag{25}$$

and the quantity $\lambda_{\mathrm{s}} = k_\perp v_{\mathrm{s}\perp}/\omega_{cs}$. It holds $w_{\mathrm{s}\perp} = v_{\mathrm{s}\perp}$, $l_{\mathrm{s}} = \lambda_{\mathrm{s}}$, $a_{\mathrm{s}} = A_{\mathrm{s}} = \tilde{A}_{\mathrm{s}}$, $y_{sn} = \eta_{sn}$, and the tensor $\mathbf{Q}_{\mathrm{s}}$ (21) takes the form (cf. Ref. 21)

$$\begin{aligned}\mathbf{Q}_{\mathrm{s}} = &\begin{pmatrix} A_{\mathrm{s}}-1 & 0 & (1-A_{\mathrm{s}})\frac{k_\perp}{k_\parallel} \\ 0 & A_{\mathrm{s}}-1 & 0 \\ (1-A_{\mathrm{s}})\frac{k_\perp}{k_\parallel} & 0 & \frac{\omega^2}{k_\parallel^2 v_{\mathrm{s}\parallel}^2} + (A_{\mathrm{s}}-1)\frac{k_\perp^2}{k_\parallel^2} \end{pmatrix} \\ &+A_{\mathrm{s}} \sum_{n=-\infty}^{\infty} \tilde{\xi}_{sn} Z(\xi_{sn}) \\ &\times \begin{pmatrix} \frac{n^2}{\lambda_{\mathrm{s}}^2}\Lambda_n & in\Lambda_n' & \frac{n}{\lambda_{\mathrm{s}}}\eta_{sn}\Lambda_n \\ -in\Lambda_n' & \frac{n^2}{\lambda_{\mathrm{s}}^2}\Lambda_n - 2\lambda_{\mathrm{s}}^2\Lambda_n' & -i\lambda_{\mathrm{s}}\eta_{sn}\Lambda_n' \\ \frac{n}{\lambda_{\mathrm{s}}}\eta_{sn}\Lambda_n & i\lambda_{\mathrm{s}}\eta_{sn}\Lambda_n' & \eta_{sn}^2\Lambda_n \end{pmatrix}\end{aligned} \tag{26}$$

where Λ_n is the scaled Bessel function of the second kind, $\Lambda_n(x) = \mathrm{e}^{-x} I_n(x)$ (I_n is the Bessel function of the second kind) and Λ_n' is its derivative,

$$\eta_{sn} = \frac{\omega - n\omega_{cs}}{k_\parallel v_{\mathrm{s}\perp}}, \tag{27}$$

$$\tilde{\xi}_{sn} = \frac{\omega - n\omega_{cs}(1-A_{\mathrm{s}}^{-1}) - k_\parallel v_{0\mathrm{s}\parallel}}{\sqrt{2}k_\parallel v_{\mathrm{s}\parallel}} = \xi_{sn} + \frac{n\omega_{cs} v_{\mathrm{s}\parallel}}{\sqrt{2}k_\parallel v_{\mathrm{s}\perp}^2}. \tag{28}$$

D. Dispersion tensor for ring distribution function 1

Let us apply the above given formulae for ring distribution function 1. Its perpendicular part (cf. Eq. (5)) is given by

$$f_{\mathrm{s}\perp}(v_\perp) = \mathrm{e}^{-\frac{v_\perp^2}{2v_{\mathrm{s}\perp}^2}} I_0\left(\frac{v_\perp v_{0\mathrm{s}\perp}}{v_{\mathrm{s}\perp}^2}\right) \tag{29}$$

where $v_{0\mathrm{s}\perp}$ represents the velocity spread of the ring. Here we use a generalized version with different thermal velocities parallel and perpendicular with respect to the ambient magnetic field. In this case we have

$$w_{\mathrm{s}\perp} = v_{\mathrm{s}\perp}\mathrm{e}^{\frac{1}{2}r_{\mathrm{s}}}, \quad \tilde{A}_{\mathrm{s}} = (1+r_{\mathrm{s}})A_s, \tag{30}$$

where $r_{\mathrm{s}} = v_{0\mathrm{s}\perp}^2/(2v_{\mathrm{s}\perp}^2)$ and A_{s} is the equivalent of the temperature anisotropy in the bi-Maxwellian case given by Eq. (25).

For the distribution (29) the integrals $S_{nmj}^{(\mathrm{s})}$ given by Eq. (14) can be expressed by Kampé de Fériet functions (defined in Appendix C),

$$\begin{aligned}S_{nmj}^{(\mathrm{s})} = &\mathrm{e}^{-\frac{j+1}{2}r_{\mathrm{s}}}\left(\frac{\lambda_{\mathrm{s}}}{\sqrt{2}}\right)^{n+m}\frac{\Gamma(\frac{n+m+j+1}{2})}{n!m!} \\ &\times F_{\cdot 13}^{1\cdot 2}\left(\begin{matrix}\frac{n+m+j+1}{2};;\frac{n+m+1}{2},\frac{n+m+2}{2} \\ ;1;n+1,m+1,n+m+1\end{matrix}\middle| r_{\mathrm{s}}, -2\lambda_{\mathrm{s}}^2\right).\end{aligned} \tag{31}$$

The sigmas defined by Eqs. (14) and (17) which are needed for the dispersion tensor can be further simplified. The final results can be found in Appendix E.

E. Dispersion tensor for ring distribution function 2

The perpendicular part of the usual, ad hoc ring distribution function (cf. Eq. (2)), denoted here as ring distribution function 2, reads

$$f_{\mathrm{s}\perp}(v_\perp) = \mathrm{e}^{-\frac{v_\perp^2}{2v_{\mathrm{s}\perp}^2}}\mathrm{e}^{\frac{v_\perp v_{0\mathrm{s}\perp}}{v_{\mathrm{s}\perp}^2}}. \tag{32}$$

For this distribution one gets

$$w_{\mathrm{s}\perp} = v_{\mathrm{s}\perp}\left[1+\sqrt{\pi}\tilde{r}_{\mathrm{s}}\mathrm{e}^{\tilde{r}_{\mathrm{s}}^2}(1+\operatorname{erf}\tilde{r}_{\mathrm{s}})\right]^{\frac{1}{2}}, \tag{33}$$

$$\tilde{A}_{\mathrm{s}} = A_{\mathrm{s}}\frac{1+\tilde{r}_{\mathrm{s}}^2+\sqrt{\pi}\tilde{r}_{\mathrm{s}}\left(\frac{3}{2}+\tilde{r}_{\mathrm{s}}^2\right)\mathrm{e}^{\tilde{r}_{\mathrm{s}}^2}(1+\operatorname{erf}\tilde{r}_{\mathrm{s}})}{1+\sqrt{\pi}\tilde{r}_{\mathrm{s}}\mathrm{e}^{\tilde{r}_{\mathrm{s}}^2}(1+\operatorname{erf}\tilde{r}_{\mathrm{s}})}, \tag{34}$$

where erf is the error function and $\tilde{r}_{\mathrm{s}} = v_{0\mathrm{s}\perp}/(v_{\mathrm{s}\perp}\sqrt{2})$.

For the distribution (32) the integrals $S_{nmj}^{(\mathrm{s})}$ given by Eq. (14) can be expressed by (modified) Kampé de Fériet functions (defined in Appendix D),

$$\begin{aligned}S_{nmj}^{(\mathrm{s})} = &\left(\frac{v_{\mathrm{s}\perp}}{w_{\mathrm{s}\perp}}\right)^{j+1}\left(\frac{\lambda_{\mathrm{s}}}{\sqrt{2}}\right)^{n+m}\frac{\Gamma(\frac{n+m+j+1}{2})}{n!m!} \\ &\times \bar{F}_{\cdot\cdot 3}^{1\cdot 2}\left(\begin{matrix}\frac{n+m+j+1}{2};;\frac{n+m+1}{2},\frac{n+m+2}{2} \\ ;;n+1,m+1,n+m+1\end{matrix}\middle| 2\tilde{r}_{\mathrm{s}}, -2\lambda_{\mathrm{s}}^2\right),\end{aligned} \tag{35}$$

The sigmas defined by Eqs. (14) and (17) which are needed for the dispersion tensor can be further simplified as in the previous case. The final results can be found in Appendix F.

Finally, in the limit $v_{0\mathrm{s}\perp} \to 0$ both ring distributions tend to a bi-Maxwellian distribution. One can easily check that it is true for the dispersion tensors, too.

IV. NUMERICAL RESULTS

Now we consider an example of instabilities driven by ring distributions. We have a three-component plasma with electrons (subscript e), core protons (subscript p),

and ring-beam protons (subscript r), drifting with respect to each other, with $n_p = 0.99\,n_e$, $n_r = 0.01\,n_e$. The ratio between the electron plasma frequency and the electron cyclotron frequency is $\omega_{pe}/\omega_{ce} = 100$. Electrons and core protons are assumed to have isotropic Maxwellian distributions with $\beta_e = \beta_p = 0.5$. Two cases of ring-beam protons are considered, the second case having a higher beta and a lower effective anisotropy. Values for the second case are given in parentheses if different. The ring-beam protons have a parallel beta $\beta_{r\parallel} = 0.005$ (0.02 in case 2). The parallel velocities of the three species are $v_{0e\parallel} = 0$, $v_{0p\parallel} = -0.02\,v_A$, $v_{0r\parallel} = 1.98\,v_A$ where the Alfvén velocity $v_A = B_0/(\mu_0 n_e m_p)^{1/2}$ (μ_0 is the vacuum permeability). The ring-beam is described by ring distributions 1 or 2 with the ring (perpendicular) velocity $v_{0r\perp} = 2\,v_A$ (in both cases) or $v_{0r\perp} \approx 1.936\,v_A$ ($1.746\,v_A$ in case 2), respectively. It ensures that the effective anisotropy $\tilde{A}_r$ of the ring distributions is the same and equal to 9 (3 in case 2). The results for the two ring distribution functions are compared with the corresponding bi-Maxwellian plasma where the ring-beam is replaced by a bi-Maxwellian beam population with the anisotropy $A_r = T_\perp/T_\parallel = 9$ (3 in case 2) and the same drift velocity $v_{0r\parallel}$.

Figure 1 compares three proton distribution functions, their perpendicular cuts $f_r(v_{0r\parallel}, v_\perp)$ (i.e., a cut through the maximum). The left panel displays case 1 whereas the right panel case 2. Figure 1 shows that for the chosen parameters the two ring distributions are very similar except for lower $v_\perp$ in case 2.

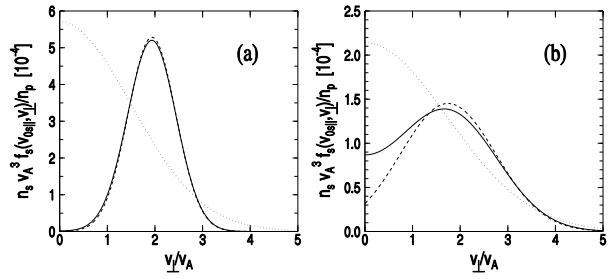

FIG. 1. Proton distribution functions in perpendicular $f_r(v_{0r\parallel}, v_\perp)$ cuts for (a) case 1 and (b) case 2. The solid and dashed lines denote ring distributions 1 and 2, respectively, the dotted lines are for the bi-Maxwellian beam distribution.

Ring-beam (as well as anisotropic beam) distributions are a source of free energy for many different instabilities driven either by the differential velocity or by the (effective) temperature anisotropy[17]. In the present case these distributions are unstable with respect to two different instabilities. The differential velocity destabilizes magnetosonic waves with the most unstable mode at oblique propagation with respect to the ambient magnetic field (this is so called oblique magnetosonic instability[22]), the unstable modes propagate (obliquely) along the beam. The temperature anisotropy of the ring (beam) destabilizes proton cyclotron waves with the maximum growth rate at the parallel direction with respect to the ambient magnetic field (ion/proton cyclotron instability). The unstable modes propagate against the ring-beam.

The dominant instability is the proton cyclotron one. Figure 2 shows the real frequency and the damping/growth rate as a function of wave vector for $\theta_{kB} = 0°$ and $\theta_{kB} = 65°$ for case 1. The maximum growth rate is $\gamma_{\max} \sim 0.026\,\omega_{cp}$ at $k \sim 0.29\,\omega_{pp}/c$ at the parallel direction. At the parallel direction all the three distributions give the same linear prediction (the linear dispersion at the parallel direction depends only on the effective temperature anisotropy in the case of separable distribution functions). At the oblique propagation the two ring distributions give almost the same linear predictions: the proton cyclotron waves have stronger growth rates than that driven by the corresponding anisotropic bi-Maxwellian beam. This is further confirmed in Figure 3 where unstable regions are shown for the ring-beam distributions and the anisotropic beam one. For both two panels the unstable region follows roughly $k_\parallel \sim 0.3\,\omega_{pp}/c$. The growth rate maximizes at the parallel direction and decreases with θ_{kB} with a slower decrease for the two ring distribution functions.

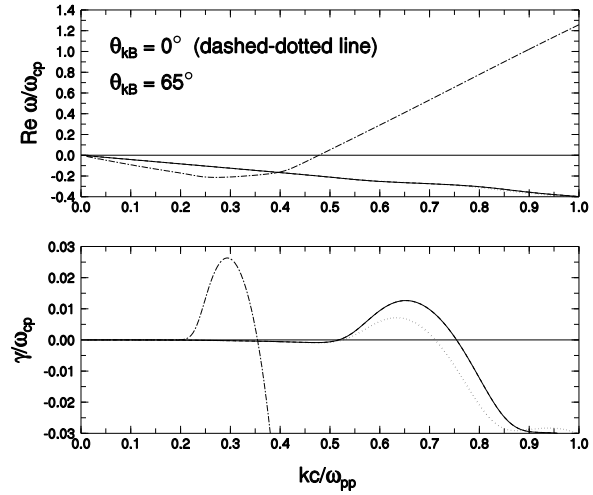

FIG. 2. Linear dispersion of the proton cyclotron instability propagating against the ring-beam for case 1: real frequency (top) and damping/growth rate (bottom) as functions of the wave vector magnitude k for $\theta_{kB} = 65°$. The solid lines are for cases when ring distributions 1 and 2 are used; they practically coincide in the plots. The dotted lines are for the case of the corresponding bi-Maxwellian anisotropic beam. In the upper plot, the solid and dotted lines nearly overlap each other. In addition, the plots are supplemented by the linear dispersion for $\theta_{kB} = 0°$ (thin dashed-dotted lines) which is the same for all the three distributions.

The oblique magnetosonic instability is subdominant, and again the two ring distributions give almost the same results. Figure 4 shows the real frequency and the damping/growth rate as a function of k for $\theta_{kB} = 43°$, the approximate angle of the most unstable mode, for the

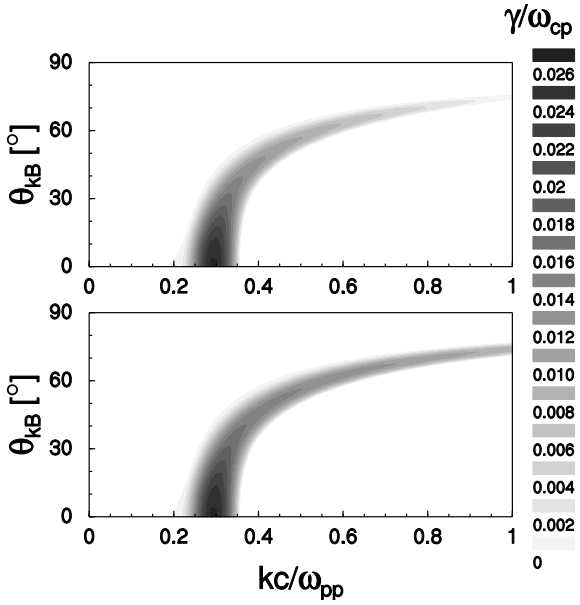

FIG. 3. Contour plots of unstable regions with respect to the proton cyclotron instability in case 1, positive γ as a function of k and θ_{kB} for (top) the anisotropic bi-Maxwellian beam and (bottom) ring distributions 1 or 2. In the latter case, the contour plots are practically the same for both distributions, so only one is shown.

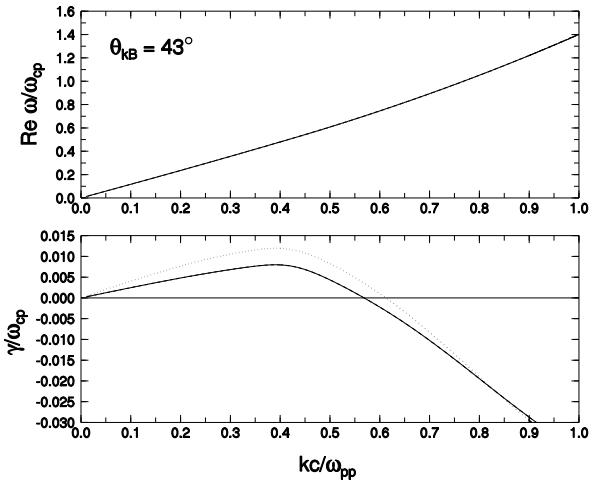

FIG. 4. Linear dispersion of the oblique magnetosonic instability propagating (obliquely) along the ring-beam in case 1: real frequency (top) and damping/growth rate (bottom) as functions of the wave vector magnitude k for the propagating angle $\theta_{kB} = 43^\circ$. The solid lines are for cases when ring distributions 1 and 2 are used, they practically coincide in the plots. The dotted lines are for the case of the corresponding bi-Maxwellian anisotropic beam. In the upper plot, all lines nearly overlap each other.

ring-beam and anisotropic beam distributions in case 1. The maximum growth rate appears at $k \sim 0.39\,\omega_{pp}/c$, the mode is more strongly unstable for the anisotropic beam distribution with the maximum growth rate $\gamma_{\max} \sim 0.012\,\omega_{cp}$ whereas for the two ring-beam distribution functions the most unstable mode has $\gamma_{\max} \sim 0.008\,\omega_{cp}$.

Figure 5 shows the unstable regions for the anisotropic beam and ring-beam distributions. The unstable region for the anisotropic beam is similar but larger that that for the ring-beam distributions.

In case 1 the linear predictions for the two ring distributions are almost identical, but in case 2 there are clear differences between two linear predictions at oblique propagation. As in the previous case, the dominant instability is the proton cyclotron one with the maximum growth rate at the parallel propagation with $\gamma_{\max} \sim 0.0038\,\omega_{cp}$ at $k \sim 0.21\,\omega_{pp}/c$, see Figure 6.

Figure 6 shows the unstable regions, a positive growth rate as a function of k and θ_{kB}, (top) for the corresponding bi-Maxwellian case, (middle) for ring distribution 1, and (bottom) for ring distribution 2. There are noticeable differences between all the linear predictions for the three different distributions at oblique propagation. In all three cases there is a local/secondary maximum (lmax) at an angle oblique with respect to the magnetic field. The secondary maximum for the bi-Maxwellian case is $\gamma_{\rm lmax} \sim 0.00076\,\omega_{cp}$ at $k \sim 0.31\,\omega_{pp}/c$ and $\theta \sim 50^\circ$, for ring distribution 1 $\gamma_{\rm lmax} \sim 0.0012\,\omega_{cp}$ at $k \sim 0.38\,\omega_{pp}/c$ and $\theta \sim 57^\circ$, and for ring distribution 2 $\gamma_{\rm lmax} \sim 0.0013\,\omega_{cp}$ at $k \sim 0.39\,\omega_{pp}/c$ and $\theta \sim 58^\circ$. Figure 6 is completed by Figure 7 which shows the real frequency and the damping/growth rate as a function of the wave vector for $\theta_{kB} = 50^\circ$ for case 2. The differences between the two ring distributions are clearly visible.

Similarly for the subdominant oblique magnetosonic instability the linear predictions for the two ring distributions are different. Figure 8 displays a positive growth rate as a function of k and θ_{kB}, (top) for the corresponding bi-Maxwellian case, (middle) for ring distribution 1, and (bottom) for ring distribution 2. The maximum growth rate for the bi-Maxwellian distribution is $\gamma_{\max} \sim 0.00089\,\omega_{cp}$ and appears at $k \sim 0.28\,\omega_{pp}/c$ and $\theta \sim 42^\circ$. For ring distribution 1 the maximum growth rate is $\gamma_{\max} \sim 0.00034\,\omega_{cp}$ at $k \sim 0.26\,\omega_{pp}/c$ and $\theta \sim 43^\circ$ whereas for ring distribution 2 the maximum growth rate is $\gamma_{\max} \sim 0.00028\,\omega_{cp}$ at $k \sim 0.25\,\omega_{pp}/c$ and $\theta \sim 43^\circ$. The differences between the two ring distribution functions are not clearly visible from Figure 8. To amend this, Figure 9 shows the real frequency and the damping/growth rate as a function of wave vector for $\theta_{kB} = 43^\circ$ for case 2. On this figure the differences between the two ring distributions are clearly seen.

These results indicate that larger differences in dispersion properties between ring distributions 1 and 2 occur for lower effective anisotropies. We investigated the dispersion properties in more detail for the oblique magnetosonic instability case. Figure 10 shows the maximum grow rates $\gamma_{\max}$ as functions of the effective temperature anisotropy $A_{\rm s}$ for the two ring distributions in two cases: the velocity $v_{0{\rm s}\perp}$ for ring distribution 1 was kept constant

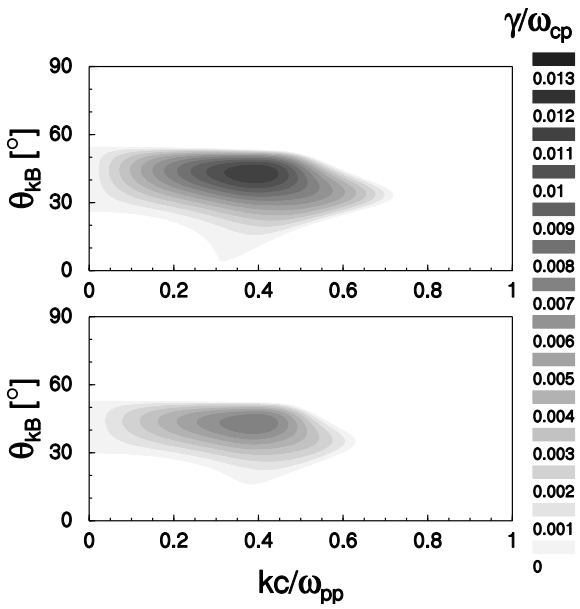

FIG. 5. Contour plots of unstable regions with respect to the oblique magnetosonic instability for case 1, positive γ as a function of k and θ_{kB} for (top) the anisotropic bi-Maxwellian beam and (bottom) ring distributions 1 or 2. In the latter case, the contour plots are practically the same for both distributions, so only one is shown.

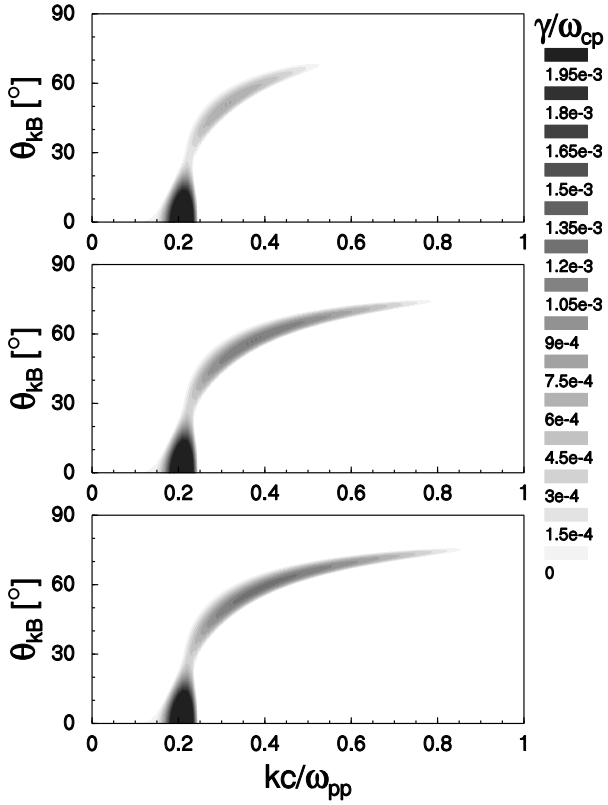

FIG. 6. Contour plots of unstable regions with respect to the proton cyclotron instability in case 2, positive γ as a function of k and θ_{kB} for (top) the anisotropic bi-Maxwellian beam, (middle) ring distribution 1, and (bottom) ring distribution 2.

for two values $v_{0s\perp} = 2\,v_A$ and $3\,v_A$ and other parameters were determined from $\tilde{A}_s$ keeping the thermal velocities $v_{s\perp} = v_{s\parallel}$ the same for the two ring distributions as in the case study above. Figure 10 demonstrates that for weaker effective temperature anisotropies the differences between the two ring distributions become larger. Consequently, the oblique magnetosonic instability has different thresholds for the two ring distribution functions.

V. DISCUSSION

In this paper we investigate linear properties of ring-beam velocity distribution functions. We derived a new form of such a distribution based on physical arguments and generalized it into the formula

$$f_s(v_\parallel, v_\perp) = \frac{\mathrm{e}^{-\frac{(v_\parallel - v_{0s\parallel})^2}{2v_{s\parallel}^2} - \frac{v_\perp^2 + v_{0s\perp}^2}{2v_{s\perp}^2}}}{(2\pi)^{\frac{3}{2}} v_{s\parallel} v_{s\perp}^2} \mathrm{I}_0\left(\frac{v_\perp v_{0s\perp}}{v_{s\perp}^2}\right). \quad (36)$$

This distribution, called here ring distribution 1, has a different form compared to the usual, ad hoc ring-beam velocity distribution function, called here ring distribution 2, which has this form:

$$f_s(v_\parallel, v_\perp) = \frac{\mathrm{e}^{-\frac{(v_\parallel - v_{0s\parallel})^2}{2v_{s\parallel}^2} - \frac{(v_\perp - v_{0s\perp})^2}{2v_{s\perp}^2}}}{(2\pi)^{\frac{3}{2}} v_{s\parallel} v_{s\perp}^2 \Psi} \quad (37)$$

where

$$\Psi = \mathrm{e}^{-\frac{v_{0s\perp}^2}{2v_{s\perp}^2}} + \sqrt{\frac{\pi}{2}} \frac{v_{0s\perp}}{v_{s\perp}} \left[1 + \mathrm{erf}\left(\frac{v_{0s\perp}}{\sqrt{2} v_{s\perp}}\right)\right]. \quad (38)$$

The two distribution functions are generally different but for a wide range of parameters they look similar for the same (effective) temperature anisotropy.

We derived the linear dispersion tensor for the two different ring velocity distribution functions in a closed form involving generalized double hypergeometric or Kampé de Fériet functions. In passing, we derived some general expressions for separable velocity distribution functions. The expressions for ring distribution 1 have a somewhat simpler form compared to those for ring distribution 2.

For a plasma consisting of isotropic Maxwellian (core) protons and electrons and a small population of ring protons drifting with respect to the core protons we compared linear dispersion properties of the two different ring distributions. For the chosen parameters the system is unstable with respect to two instabilities. The dominant one is the proton cyclotron instability driven by the (effective) temperature anisotropy of the ring population with the most unstable mode at the parallel direction with respect to the ambient magnetic field. The sub-

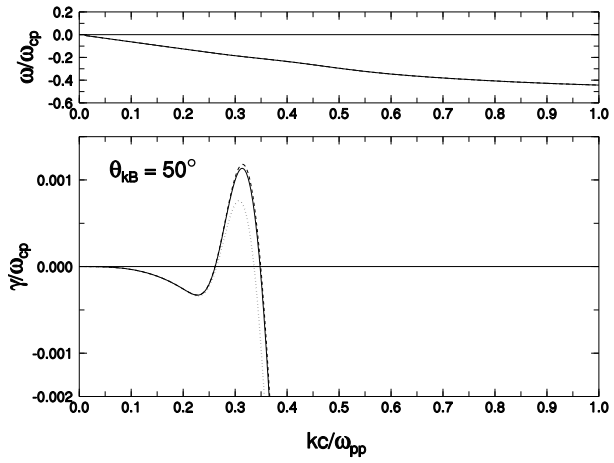

FIG. 7. Linear dispersion of the proton cyclotron instability propagating against the ring-beam for case 2: real frequency (top) and damping/growth rate (bottom) as functions of the wave vector magnitude k for $\theta_{kB} = 50°$. The solid and dashed lines are for cases when ring distributions 1 and 2 are used, respectively. The dotted lines are for the case of the corresponding bi-Maxwellian anisotropic beam. In the upper plot, all lines nearly overlap each other.

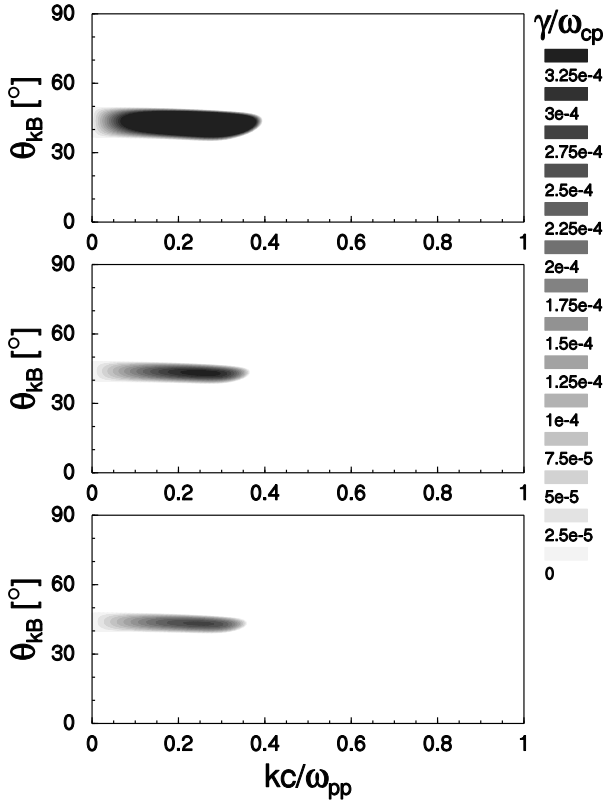

FIG. 8. Contour plots of unstable regions with respect to the oblique magnetosonic instability for case 2, positive γ as a function of k and θ_{kB} for (top) the anisotropic bi-Maxwellian beam, (middle) ring distribution 1, and (bottom) ring distribution 2.

dominant is the oblique magnetosonic instability driven by the differential velocity between the core and ring protons and has the most unstable mode at oblique propagation. For large (effective) temperature anisotropies the two ring distributions give essentially the same linear results. However, for weaker anisotropies (and weaker growth rates) the two linear predictions differ at oblique propagation. At the parallel direction the two distributions are equivalent to each other for the same effective temperature anisotropy (and they are equivalent to the corresponding distribution where the ring is replaced by a bi-Maxwellian distribution with the same temperature anisotropy). The difference between the two linear predictions (at oblique propagation) increases with decrease of the effective temperature anisotropy. In particular, the oblique magnetosonic instability has generally different thresholds for the two ring distributions. Such an important dependence of marginal stability on the distribution function is likely a general feature of resonant instabilities[17] where the linear dispersion properties are dominated by one resonance $\propto 1/(\omega - k_\parallel v_\parallel - n\omega_{cs})$; this resonance becomes very localized (in $v_\parallel$) for weak growth rates, $\gamma \to 0$.

The present results are relevant for the outer heliosheath where hot ring distribution functions are expected. The analysis of Ref. 9 indicates that a sufficient thermal spread for the ad hoc ring distribution may linearly stabilize the system making these ions possible source of the observed energetic neutrals.[7]. This property likely holds for the physics-based ring distribution as well, but the linear stability conditions for these two distributions are different. Further work is needed to determine the stability of the hot ring distribution functions in the context of the outer heliosheath. The source of outer heliosheath ring ions, hot neutrals of the solar wind origin, is likely to have a distribution function more complicated than the Maxwellian one assumed in Section II so that it will probably be necessary to extend the physics-based model (Eq. (36)) and the analytical linear dispersion analysis following the procedure presented here.

Appendix A: General relationships

Quantities $R^{(s)}_{nmj}$ given by Eq. (13) are not independent and various relationships were used during the calcula-

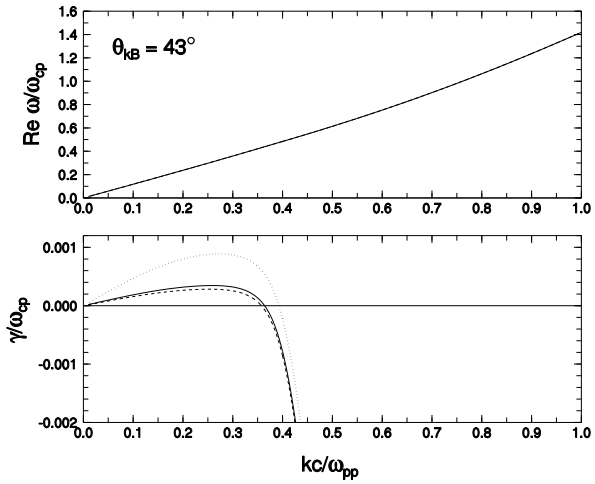

FIG. 9. Linear dispersion of the oblique magnetosonic instability propagating (obliquely) along the ring-beam in case 2: real frequency (top) and damping/growth rate (bottom) as functions of the wave vector magnitude k for the propagating angle $\theta_{kB} = 43^\circ$. The solid and dashed lines are for cases when ring distributions 1 and 2 are used, respectively. The dotted lines are for the case of the corresponding bi-Maxwellian anisotropic beam. In the upper plot, all lines nearly overlap each other.

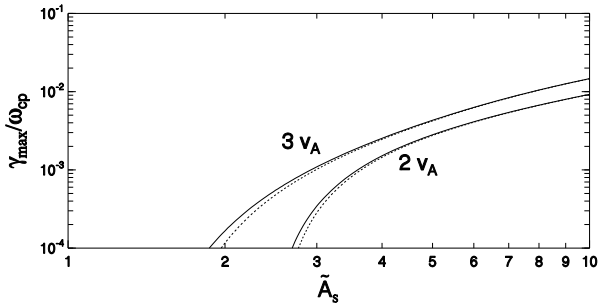

FIG. 10. Comparison between the two ring distributions for the oblique magnetosonic instability: Maximum grow rates $\gamma_{\max}$ as functions of the effective temperature anisotropy $\tilde{A}_\mathrm{s}$ in a log-log scale for ring distribution 1 (solid lines) and ring distribution 2 (dashed lines) in two cases: for the ring velocity (corresponding to the ring distribution 1) $v_{0\mathrm{s}\perp} = 2\,v_A$ (bottom curves) and $v_{0\mathrm{s}\perp} = 3\,v_A$ (upper curves).

tions, namely

$$\begin{aligned}
R^{(\mathrm{s})}_{000} &= \sqrt{2},\\
R^{(\mathrm{s})}_{n11} &= R^{(\mathrm{s})}_{000} + \frac{w_{\mathrm{s}\perp}}{w_{\mathrm{s}\parallel}} y_{sn} R^{(\mathrm{s})}_{n10},\\
R^{(\mathrm{s})}_{n22} &= R^{(\mathrm{s})}_{000} + 2\frac{w_{\mathrm{s}\perp}}{w_{\mathrm{s}\parallel}} y_{sn} R^{(\mathrm{s})}_{n21} - \frac{w^2_{\mathrm{s}\perp}}{w^2_{\mathrm{s}\parallel}} y^2_{sn} R^{(\mathrm{s})}_{n20},\\
R^{(\mathrm{s})}_{n21} &= R^{(\mathrm{s})}_{n10} + \frac{w_{\mathrm{s}\perp}}{w_{\mathrm{s}\parallel}} y_{sn} R^{(\mathrm{s})}_{n20},\\
R^{(\mathrm{s})}_{n12} &= R^{(\mathrm{s})}_{001} + \frac{w_{\mathrm{s}\perp}}{w_{\mathrm{s}\parallel}} y_{sn} R^{(\mathrm{s})}_{n11}.
\end{aligned} \tag{A1}$$

It holds

$$\begin{aligned}
S^{(\mathrm{s})}_{nmj} &= (-1)^n S^{(\mathrm{s})}_{-n,m,j},\\
S^{(\mathrm{s})}_{nmj} &= (-1)^m S^{(\mathrm{s})}_{n,-m,j},\\
S^{(\mathrm{s})}_{nmj} &= (-1)^{n+m} S^{(\mathrm{s})}_{-n,-m,j},
\end{aligned} \tag{A2}$$

therefore all sigmas defined by Eqs. (17) are even in n, $\sigma_{ls n} = \sigma_{ls|n|}$, so $\sum_n n\sigma_{1sn} = 0$ etc. Here $\sum_n$ is a shorthand for $\sum_{n=-\infty}^{\infty}$. Some other sums can be evaluated,

$$\begin{aligned}
&2\sum_n \sigma_{1sn} = \sum_n \sigma_{4sn} = \sum_n n^2 \sigma_{8sn} = 2,\\
&\sum_n \sigma_{2sn} = \sum_n \sigma_{3sn} = \sum_n \sigma_{5sn} = \sum_n \sigma_{8sn} = 0,\\
&\sum_n n^2 \sigma_{2sn} = \sqrt{2} l_\mathrm{s},
\end{aligned} \tag{A3}$$

which follow from the definitions of sigmas and summation identities for the Bessel functions, e.g., $\sum_n J^2_n(x) = 1$, $\sum_n n^2 J^2_n(x) = x^2/2$, $\sum_n J'^2_n(x) = 1/2$, etc.

Appendix B: Relationships for the streaming Maxwellian parallel distribution function

When the parallel distribution function is given by Eq. (18), additional summation identities can be expressed as

$$\begin{aligned}
&\sum_n n^2 \sigma_{1sn} = \sum_n n^2 \sigma_{5sn} = \frac{l^2_\mathrm{s}}{a_\mathrm{s}} \tilde{A}_\mathrm{s} = \sum_n n^2 \sigma_{4sn} - 2,\\
&\sum_n n^2 \sigma_{3sn} = \frac{\sqrt{2} l_\mathrm{s}}{a_\mathrm{s}} \tilde{A}_\mathrm{s}, \qquad \sum_n \sigma_{7sn} = \frac{2\tilde{A}_\mathrm{s}}{a_\mathrm{s}}.
\end{aligned} \tag{B1}$$

Appendix C: Kampé de Fériet functions

The Kampé de Fériet functions are generalized hypergeometric functions with two arguments[23] and are defined by series. Here we make use of two types:

$$F^{1\cdot 1}_{\cdot 12}\left(\begin{matrix} a;;b \\ ;c;d,e \end{matrix} \middle| x, y \right) = \sum_{k,l=0}^{\infty} \frac{(a)_{k+l}(b)_l}{(c)_k (d)_l (e)_l} \frac{x^k}{k!} \frac{y^l}{l!}, \tag{C1}$$

$$F^{1\cdot2}_{\cdot13}\left(\begin{matrix}a;;b,c\\;d;e,f,g\end{matrix}\middle|x,y\right)=\sum_{k,l=0}^{\infty}\frac{(a)_{k+l}(b)_l(c)_l}{(d)_k(e)_l(f)_l(g)_l}\frac{x^k}{k!}\frac{y^l}{l!},\tag{C2}$$

$(a)_n$ is the rising factorial (Pochhammer symbol), $(a)_n = \Gamma(n+a)/\Gamma(a)$, Γ is the gamma function.

Appendix D: Modified Kampé de Fériet functions

In the derivation of dispersion relations for the ring 2 distribution function one arrives at functions here denoted as $\bar{F}$ which are not the Kampé de Fériet functions, but they are defined by similar series,

$$\bar{F}^{1\cdot1}_{\cdot\cdot2}\left(\begin{matrix}a;;b\\;;c,d\end{matrix}\middle|x,y\right)=\sum_{k,l=0}^{\infty}\frac{(a)_{\frac{k}{2}+l}(b)_l}{(c)_l(d)_l}\frac{x^k}{k!}\frac{y^l}{l!},\tag{D1}$$

$$\bar{F}^{1\cdot2}_{\cdot\cdot3}\left(\begin{matrix}a;;b,c\\;;d,e,f\end{matrix}\middle|x,y\right)=\sum_{k,l=0}^{\infty}\frac{(a)_{\frac{k}{2}+l}(b)_l(c)_l}{(d)_l(e)_l(f)_l}\frac{x^k}{k!}\frac{y^l}{l!}\tag{D2}$$

which can be expressed by the Kampé de Fériet functions in this way:

$$\begin{aligned}\bar{F}^{1\cdot1}_{\cdot\cdot2}\left(\begin{matrix}a;;b\\;;c,d\end{matrix}\middle|x,y\right)&=F^{1\cdot1}_{\cdot12}\left(\begin{matrix}a;;b\\;\frac{1}{2};c,d\end{matrix}\middle|\frac{x^2}{4},y\right)\\&+x\frac{\Gamma\left(a+\frac{1}{2}\right)}{\Gamma(a)}F^{1\cdot1}_{\cdot12}\left(\begin{matrix}a+\frac{1}{2};;b\\;\frac{3}{2};c,d\end{matrix}\middle|\frac{x^2}{4},y\right),\end{aligned}\tag{D3}$$

$$\begin{aligned}\bar{F}^{1\cdot2}_{\cdot\cdot3}\left(\begin{matrix}a;;b,c\\;;d,e,f\end{matrix}\middle|x,y\right)&=F^{1\cdot2}_{\cdot13}\left(\begin{matrix}a;;b,c\\;\frac{1}{2};d,e,f\end{matrix}\middle|\frac{x^2}{4},y\right)\\&+x\frac{\Gamma\left(a+\frac{1}{2}\right)}{\Gamma(a)}F^{1\cdot2}_{\cdot13}\left(\begin{matrix}a+\frac{1}{2};;b,c\\;\frac{3}{2};d,e,f\end{matrix}\middle|\frac{x^2}{4},y\right).\end{aligned}\tag{D4}$$

To obtain the expressions (D3)–(D4), summations by k in Eqs. (D1)–(D2) were split into even and odd numbers and simplified using these two identities: $(2n)! = 2^{2n}n!(1/2)_n$, $(2n+1)! = 2^{2n}n!(3/2)_n$.

Even though $\bar{F}$ functions can be expressed by the Kampé de Fériet functions, we introduced them because then formulae and their derivations are very similar for both ring distributions (cf. Eqs. (31) and (35), or Appendices E and F).

Appendix E: Ring distribution 1

The sigmas defined by Eqs. (17) can be simplified for the ring distribution function 1 (Section III D):

$$\begin{aligned}\sigma_{1sn}&=\frac{\mathrm{e}^{-r_\mathrm{s}}}{n!}\left(\frac{\lambda_\mathrm{s}}{\sqrt{2}}\right)^{2n}F_1(n,1,1),\\\sigma_{2sn}&=\frac{\mathrm{e}^{-\frac{1}{2}r_\mathrm{s}}}{n!}\left(\frac{\lambda_\mathrm{s}}{\sqrt{2}}\right)^{2n-1}F_1(n,0,0),\\\sigma_{3sn}&=\frac{\mathrm{e}^{-\frac{3}{2}r_\mathrm{s}}}{(n-1)!}\left(\frac{\lambda_\mathrm{s}}{\sqrt{2}}\right)^{2n-1}F_1(n,1,0),\\\sigma_{7sn}&=\frac{\mathrm{e}^{-2r_\mathrm{s}}}{(n-1)!}\left(\frac{\lambda_\mathrm{s}}{\sqrt{2}}\right)^{2n-2}\\&\quad\times\left[nF_1(n,1,1)-2\lambda_\mathrm{s}^2F_2(n,2,2)\right],\\\sigma_{8sn}&=\frac{\mathrm{e}^{-r_\mathrm{s}}}{(n-1)!}\left(\frac{\lambda_\mathrm{s}}{\sqrt{2}}\right)^{2n-2}F_2(n,0,0),\\\sigma_{9sn}&=\frac{\mathrm{e}^{-\frac{3}{2}r_\mathrm{s}}}{(n-1)!}\left(\frac{\lambda_\mathrm{s}}{\sqrt{2}}\right)^{2n-3}\\&\quad\times\left[nF_1(n,0,0)-2\lambda_\mathrm{s}^2F_1(n,1,0)\right]\end{aligned}\tag{E1}$$

where F_1 and F_2 are given by the Kampé de Fériet functions $F^{1\cdot1}_{\cdot12}$ and $F^{1\cdot2}_{\cdot13}$ defined in Appendix C,

$$\begin{aligned}F_1(n,k,l)&=F^{1\cdot1}_{\cdot12}\left(\begin{matrix}n+k;;n+\frac{1}{2}\\;1;n+l,2n+1\end{matrix}\middle|r_\mathrm{s},-2\lambda_\mathrm{s}^2\right),\\F_2(n,k,l)&=F^{1\cdot2}_{\cdot13}\left(\begin{matrix}n+k;;n+1,n+\frac{1}{2}\\;1;n+l,n,2n+1\end{matrix}\middle|r_\mathrm{s},-2\lambda_\mathrm{s}^2\right).\end{aligned}\tag{E2}$$

The expressions in Eqs. (E1) are not defined for $n<0$ but it holds $\sigma_{lsn}=\sigma_{ls|n|}$. The formulae for σ_{2sn}, σ_{3sn}, σ_{7sn}, σ_{8sn}, and σ_{9sn} are valid only for $n>0$, for $n=0$ we need only σ_{3sn} and σ_{7sn}, it is

$$\sigma_{3s0}=-\mathrm{e}^{-\frac{3}{2}r_\mathrm{s}}\sqrt{2}\lambda_\mathrm{s}\,F^{1\cdot1}_{\cdot12}\left(\begin{matrix}2;;\frac{3}{2}\\;1;2,2\end{matrix}\middle|r_\mathrm{s},-2\lambda_\mathrm{s}^2\right),\tag{E3}$$

$$\sigma_{7s0}=4\mathrm{e}^{-2r_\mathrm{s}}\lambda_\mathrm{s}^2\,F^{1\cdot1}_{\cdot12}\left(\begin{matrix}3;;\frac{3}{2}\\;1;2,3\end{matrix}\middle|r_\mathrm{s},-2\lambda_\mathrm{s}^2\right).\tag{E4}$$

During the calculation of (E1) Bessel functions are substituted by their series, integrals are evaluated, and multiple sums are simplified using identities

$$\sum_{l=0}^{\infty}\sum_{t=0}^{\infty}a_{lt}=\sum_{q=0}^{\infty}\sum_{p=0}^{q}a_{p,q-p}\tag{E5}$$

and

$$\sum_{p=0}^{q}\binom{n+q}{p}\binom{n+q}{q-p}=\binom{2n+2q}{q},\tag{E6}$$

the latter one as a consequence of the Vandermonde convolution. The formula (31) holds for $n\geq0$, $m\geq0$, and $j\geq0$. For negative values of n and m the relationships (A2) are used.

The expression for σ_{1sn} follows directly from Eq. (31); there are identical one upper and one corresponding lower parameters, hence the function $F^{1\cdot2}_{\cdot13}$ reduces to $F^{1\cdot1}_{\cdot12}$. The σ_{2sn} and σ_{3sn} involve similar differences in $S^{(\mathrm{s})}_{nmj}$'s and the following procedure for simplification is used:

$$\begin{aligned} &F^{1\cdot1}_{\cdot12}\left(\begin{array}{c} n+\frac{j}{2};;n+\frac{1}{2} \\ ;1;n+1,2n \end{array}\middle| x,y\right) \\ &+\frac{y}{4}\frac{n+\frac{j}{2}}{n(n+1)}F^{1\cdot1}_{\cdot12}\left(\begin{array}{c} n+1+\frac{j}{2};;n+\frac{3}{2} \\ ;1;n+2,2n+2 \end{array}\middle| x,y\right) \\ &=F^{1\cdot1}_{\cdot12}\left(\begin{array}{c} n+\frac{j}{2};;n+\frac{1}{2} \\ ;1;n,2n+1 \end{array}\middle| x,y\right). \end{aligned} \tag{E7}$$

The other sigmas are derived in similar ways. Alternative calculations of sigmas do not start with Eq. (31) but with the integral definition of $S^{(\mathrm{s})}_{nmj}$ (14). Differences of Bessel functions are expressed by their derivatives which are consequently substituted by series and calculations proceed is a similar way which was used to obtain Eq. (31).

Appendix F: Ring distribution 2

The sigmas defined by Eqs. (17) can be also simplified for the ring distribution function 2 (Section III E):

$$\begin{aligned} \sigma_{1sn} &= \left(\frac{v_{\mathrm{s}\perp}}{w_{\mathrm{s}\perp}}\right)^2\frac{1}{n!}\left(\frac{\lambda_{\mathrm{s}}}{\sqrt{2}}\right)^{2n}\bar{F}_1(n,1,1), \\ \sigma_{2sn} &= \frac{v_{\mathrm{s}\perp}}{w_{\mathrm{s}\perp}}\frac{1}{n!}\left(\frac{\lambda_{\mathrm{s}}}{\sqrt{2}}\right)^{2n-1}\bar{F}_1(n,0,0), \\ \sigma_{3sn} &= \left(\frac{v_{\mathrm{s}\perp}}{w_{\mathrm{s}\perp}}\right)^3\frac{1}{(n-1)!}\left(\frac{\lambda_{\mathrm{s}}}{\sqrt{2}}\right)^{2n-1}\bar{F}_1(n,1,0), \\ \sigma_{7sn} &= \left(\frac{v_{\mathrm{s}\perp}}{w_{\mathrm{s}\perp}}\right)^4\frac{1}{(n-1)!}\left(\frac{\lambda_{\mathrm{s}}}{\sqrt{2}}\right)^{2n-2} \\ &\quad\times\left[n\bar{F}_1(n,1,1)-2\lambda_{\mathrm{s}}^2\bar{F}_2(n,2,2)\right], \\ \sigma_{8sn} &= \left(\frac{v_{\mathrm{s}\perp}}{w_{\mathrm{s}\perp}}\right)^2\frac{1}{(n-1)!}\left(\frac{\lambda_{\mathrm{s}}}{\sqrt{2}}\right)^{2n-2}\bar{F}_2(n,0,0), \\ \sigma_{9sn} &= \left(\frac{v_{\mathrm{s}\perp}}{w_{\mathrm{s}\perp}}\right)^3\frac{1}{(n-1)!}\left(\frac{\lambda_{\mathrm{s}}}{\sqrt{2}}\right)^{2n-3} \\ &\quad\times\left[n\bar{F}_1(n,0,0)-2\lambda_{\mathrm{s}}^2\bar{F}_1(n,1,0)\right], \end{aligned} \tag{F1}$$

where $\bar{F}_1$ and $\bar{F}_2$ are given by the modified Kampé de Fériet functions (see Appendix D)

$$\bar{F}_1(n,k,l)=\bar{F}^{1\cdot1}_{\cdot\cdot2}\left(\begin{array}{c} n+k;;n+\frac{1}{2} \\ ;;n+l,2n+1 \end{array}\middle| 2\tilde{r}_{\mathrm{s}},-2\lambda_{\mathrm{s}}^2\right), \tag{F2}$$

$$\bar{F}_2(n,k,l)=\bar{F}^{1\cdot2}_{\cdot\cdot3}\left(\begin{array}{c} n+k;;n+1,n+\frac{1}{2} \\ ;;n+l,n,2n+1 \end{array}\middle| 2\tilde{r}_{\mathrm{s}},-2\lambda_{\mathrm{s}}^2\right).$$

As in the previous case (Appendix E) the expressions in Eqs. (F1) are not defined for $n<0$ but it holds $\sigma_{lsn}=\sigma_{ls|n|}$. The formulae for σ_{2sn}, σ_{3sn}, σ_{7sn}, σ_{8sn}, and σ_{9sn} are valid only for $n>0$, for $n=0$ we need only σ_{3sn} and σ_{7sn}, it is

$$\sigma_{3s0}=-\left(\frac{v_{\mathrm{s}\perp}}{w_{\mathrm{s}\perp}}\right)^3\sqrt{2}\lambda_{\mathrm{s}}\,\bar{F}^{1\cdot1}_{\cdot\cdot2}\left(\begin{array}{c} 2;;\frac{3}{2} \\ ;;2,2 \end{array}\middle| 2\tilde{r}_{\mathrm{s}},-2\lambda_{\mathrm{s}}^2\right), \tag{F3}$$

$$\sigma_{7s0}=4\left(\frac{v_{\mathrm{s}\perp}}{w_{\mathrm{s}\perp}}\right)^4\lambda_{\mathrm{s}}^2\,\bar{F}^{1\cdot1}_{\cdot\cdot2}\left(\begin{array}{c} 3;;\frac{3}{2} \\ ;;2,3 \end{array}\middle| 2\tilde{r}_{\mathrm{s}},-2\lambda_{\mathrm{s}}^2\right). \tag{F4}$$

ACKNOWLEDGMENTS

The research leading to these results has received funding from the European Commission's Seventh Framework Programme (FP7) under the grant agreement SHOCK (project number 284515, project-shock.eu). This work was also supported by grants P209/12/2023 and P209/12/2041 of the Czech Science Foundation and by projects RVO:67985815 and RVO:68378289.

* marek.vandas@asu.cas.cz

[1] A. J. Coates, A. D. Johnstone, B. Wilken, and F. M. Neubauer, J. Geophys. Res. **98**, 20985 (1993)
[2] A. L. Brinca, L. B. de Água, and D. Winske, J. Geophys. Res. **98**, 7549 (1993)
[3] C. S. Wu and R. C. Davidson, J. Geophys. Res. **77**, 5399 (1972)
[4] G. Gloeckler and J. Geiss, Space Sci. Rev. **86**, 127 (1998)
[5] J. D. Richardson, J. L. Phillips, C. W. Smith, and P. C. Gray, Geophys. Res. Lett. **23**, 3259 (1996)
[6] T. R. Detman, D. S. Intriligator, M. Dryer, W. Sun, C. S. Deehr, and J. Intriligator, J. Geophys. Res. **116**, A03105 (2011), 10.1029/2010JA15803
[7] D. J. McComas *et al.*, Science **326**, 959 (2009)
[8] V. Florinski, G. P. Zank, J. Heerikhuisen, Q. Hu, and I. Khazanov, Astrophys. J. **719**, 1097 (2010)

[9] E. J. Summerlin, A. F. Viñas, T. E. Moore, E. R. Christian, and J. F. Cooper, Astrophys. J. **793**, 93 (2014), 10.1088/0004-637X/793/2/93
[10] C. S. Wu, D. Krauss-Varban, and T. S. Huo, J. Geophys. Res. **93**, 11527 (1988)
[11] S. P. Gary and C. D. Madland, J. Geophys. Res. **93**, 235 (1988)
[12] K. Killen, N. Omidi, D. Krauss-Varban, and H. Karimabadi, J. Geophys. Res. **100**, 5835 (1995)
[13] P. C. Gray, C. W. Smith, W. H. Matthaeus, and N. F. Otani, Geophys. Res. Lett. **23**, 113 (1996)
[14] D. Winske, C. S. Wu, Y. Y. Li, Z. Z. Mou, and S. Y. Guo, J. Geophys. Res. **90**, 2713 (1985)
[15] H. K. Wong, M. L. Goldstein, and C. W. Smith, J. Geophys. Res. **96**, 285 (1991)
[16] T. Umeda, S. Matsukiyo, T. Amano, and Y. Miyoshi, Phys. Fluids **19**, 072107 (2012), 10.1063/1.4736848
[17] S. P. Gary, *Theory of Space Plasma Microinstabilities* (Cambridge Univ. Press, New York, 1993)
[18] T. H. Stix, *Waves in plasmas* (AIP, New York, 1992)
[19] B. D. Fried and S. D. Conte, *The plasma dispersion function* (Academic Press, New York, 1961)
[20] M. G. Kivelson, in *Introduction to Space Physics* (Cambridge Univ. Press, New York, 1996) pp. 36–37
[21] M. L. Goldstein, H. K. Wong, and A. F. Viñas, J. Geophys. Res. **90**, 302 (1985)
[22] W. Daughton and S. P. Gary, J. Geophys. Res. **103**, 20613 (1998)
[23] H. Exton, *Multiple hypergeometric functions and applications*, Mathematics & its Applications (Halsted Press, New York, 1976)